ARTICLES
PUBLISHED ONLINE: 28 MARCH 2010 | DOI: 10.1038/NPHOTON.2010.37
nature photonics

Amplification of long-range surface plasmons by a dipolar gain medium

Israel De Leon[1] and Pierre Berini[1,2,3]*

Surface plasmon–polaritons, collective electron oscillations coupled to light waves at the surface of a metal, show unique properties that are valuable in a broad range of scientific fields. However, the intrinsic propagation loss of these waves poses a fundamental problem to many potential applications. To overcome this drawback, researchers have explored the possibility of loss compensation by means of surface plasmon–polariton amplification. Here we provide the first direct measurement of gain in propagating plasmons using the long-range surface plasmon–polariton supported by a symmetric metal stripe waveguide that incorporates optically pumped dye molecules in solution as the gain medium. The measured mode power gain is 8.55 dB mm^{-1}. Furthermore, it is shown that this new class of amplifier benefits from reduced spontaneous emission into the amplified mode, potentially leading to low-noise optical amplification.

Surface plasmon–polaritons (SPPs) are transverse magnetic (TM) polarized optical surface waves that propagate along a metal–dielectric interface and whose fields are coupled to charge density oscillations in the metal[1]. SPPs show unique properties including strong electromagnetic field enhancement, subwavelength localization and high sensitivity to the bounding dielectric environment. Such properties make SPPs attractive for applications in fields such as nanophotonics[2], metamaterials[3], imaging[4] and biosensing[5]. However, such applications face limitations imposed by the short lifetimes of SPPs at visible and near-infrared wavelengths, caused by energy dissipation in the metal due to electron collisions and other loss mechanisms. This obstacle has stimulated great interest in understanding the physics of SPP amplification as well as exploring the feasibility of achieving SPP loss compensation using this mechanism[6–23].

The stimulated emission of SPPs has been observed for various planar plasmonic structures. Stimulated emission has been observed in an SPP supported by a silver film in the Kretschmann configuration, coated on its backside with an optically pumped dye solution[15], and in similar structures in which the gain medium comprised a dye-doped polymer[16,17]. In other research, emission has been studied in symmetrical metal-stripe waveguides clad with erbium-doped SiO_2 using a propagating pump arrangement[18]. Grandidier and colleagues[19] demonstrated a 27% increase in the SPP propagation length at telecommunication wavelengths in a quantum-dot-doped polymer-strip-loaded plasmonic waveguide, and Oulton and colleagues[20] demonstrated lasing at visible wavelengths in hybrid plasmon modes supported by a silver film coupled to a cadmium sulphide nanowire. Stimulated emission of SPPs has also been studied in metallic nanostructures. Lasing at telecommunication wavelengths has been observed in metal-coated nanocavities filled with an electrically pumped semiconductor gain medium[21,22], and coherent generation of localized SPPs has been demonstrated at visible wavelengths in an arrangement using gold nanoparticles encapsulated in dye-doped silica shells[23].

Previous studies have argued SPP gain on the basis of a theoretical interpretation of SPP stimulated emission[17] or through the observation of laser-like behaviour of light coupled out of active plasmonic structures[20–23]. In this work we report the first direct measurement of gain in propagating SPPs. The experiments were conducted using the long-range SPP (LRSPP)[24–29] supported by a symmetric gold-stripe plasmonic waveguide[30] incorporating a gain medium in the form of optically pumped dye molecules in solution. We demonstrate that the LRSPP, supported by the structure, propagates with a mode power gain of 8.55 dB mm^{-1}. Furthermore, we show that this class of amplifier benefits from low spontaneous emission into the LRSPP, potentially leading to low-noise optical amplification. We demonstrate a 6.3-dB reduction of spontaneous emission noise in the vicinity of the plasmonic waveguide relative to that in the bulk gain medium.

The realization of LRSPP amplifiers has potential in a number of applications. For instance, the integration of LRSPP amplifiers with grating structures[31,32] could lead to the development of LRSPP lasers that inherit the pure TM polarization of SPP modes, suggesting that a highly polarized output with polarization extinction ratio limited only by the spontaneous emission noise could be achieved. Also, LRSPP amplifiers and lasers could be conveniently integrated with an existing complement of passive optical components[33,34] such as four-port couplers, y-junctions, bandgap structures and Mach–Zehnder interferometers, leading to devices and components with sophisticated functionality. Finally, low-noise optical amplification would improve the performance of biosensors[35].

The LRSPP is not confined to use in very small modal dimensions (subwavelength), but it does propagate with lower loss, which reduces the material gain required to achieve modal gain. Total loss compensation in deep subwavelength SPPs still remains a challenge due to the high propagation losses present, particularly at visible and near-infrared wavelengths.

Results

Guiding structure. The plasmonic waveguides used in the present experiments were derived from wafer X023506.15 as reported in ref. 36, and the fabrication details and results of physical characterization are provided therein. A cross-sectional view of the waveguide structure is shown in Fig. 1a. The gold stripe was 20 nm thick and 1 μm wide, with a root-mean-square (r.m.s.)

[1]School of Information Technology and Engineering, University of Ottawa, 161 Louis Pasteur, Ottawa, Ontario, K1N 6N5, Canada, [2]Department of Physics, University of Ottawa, 150 Louis Pasteur, Ottawa, Ontario, K1N 6N5, Canada, [3]Spectalis Corp., PO Box 72029, Kanata North RPO, Ottawa, Ontario, K2K 2P4, Canada. *e-mail: berini@site.uottawa.ca

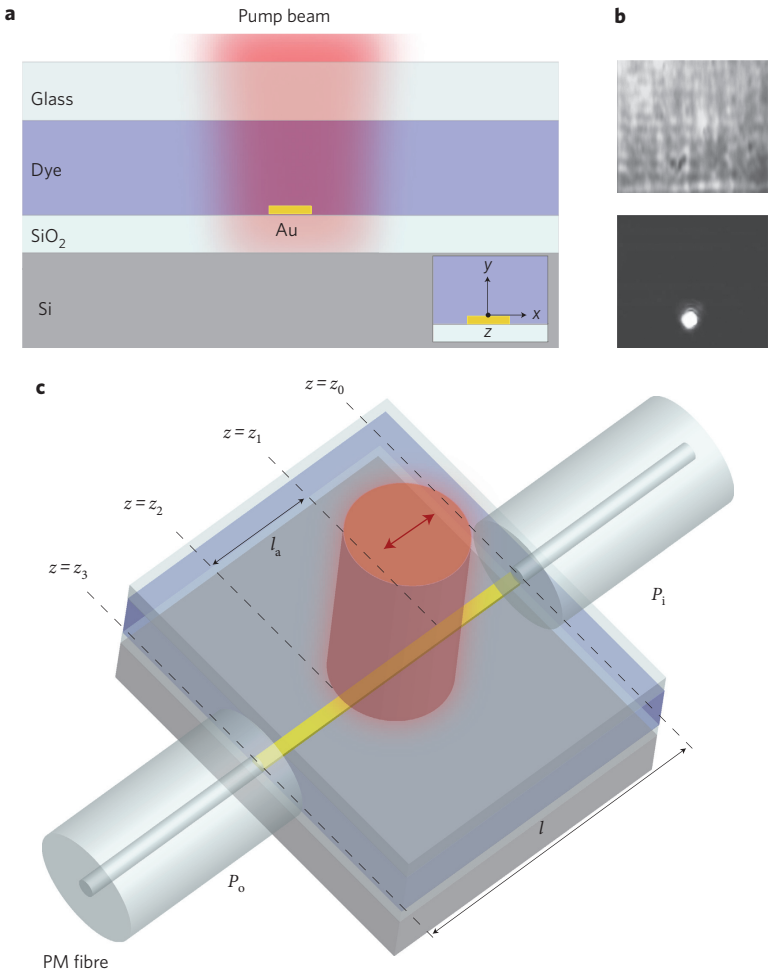

Figure 1 | Guiding structure. a, Cross-sectional view of active structure (not to scale). The gain medium is in the form of a laser dye in solution. Inset: coordinate system with the +*z*-direction coming out of the page. **b**, *x*-Polarized (top) and *y*-polarized (bottom) light collected from the output facet of the structure while being pumped by *x*-polarized light. **c**, Pump and probe signal coupling arrangements used for amplification experiments. Pump polarization, indicated by the red arrow, is parallel to the waveguide length (*z*-axis). A probe signal is coupled in and out of the structure by means of end-fire coupling using polarization-maintaining (PM) fibres.

surface roughness of less than 1 nm, and lay on a 15-μm-thick SiO_2 layer thermally grown on a silicon substrate and was covered by a gain layer ~100 μm thick consisting of optically pumped IR140 dye molecules (Sigma Aldrich) in solution. The dye was pumped at $\lambda_p = 808$ nm and the LRSPP was probed (excited) at $\lambda_e = 882$ nm, close to the peak absorption and emission of the dye, respectively (see Supplementary Information). The arrangement used for pumping and probing is depicted in Fig. 1c. The pump light was normally incident onto the top side of the structure, linearly polarized along the *z*-axis, and consisted of 8-ns FWHM (full-width at half-maximum) pulses with a repetition rate of 10 Hz. It uniformly illuminated the central region of the structure with a spot diameter smaller than the length l of the structure. The continuous-wave probe signal was coupled in and out of the LRSPP by means of end-fire coupling using polarization-maintaining fibre (see Methods).

The dye concentration was 1 mM, corresponding to a molecular density of $N = 6 \times 10^{17}$ cm^{-3}, and the solvent was a mixture of 30.4% ethylene glycol and 69.6% dimethyl sulphoxide. At a temperature of 23 °C, the dye solution was index-matched to SiO_2 at λ_e, forming a symmetric waveguiding structure. When fully inverted, the dye is expected to provide a gain of $N\sigma_e \approx 360$ cm^{-1}, with $\sigma_e \approx 6 \times 10^{16}$ being the emission cross-section at λ_e (see Supplementary Information). Figure 1b shows images of light collected from the output facet of the structure while being pumped by *x*-polarized light and with the LRSPP excited by the probe signal. For the top (bottom) image the output light is passed through a polarizer oriented along the *x* (*y*) direction. The bright spot on the bottom image corresponds to the LRSPP intensity profile. It is not visible in the top image because $E_x \approx 0$ for this mode[30]. The brightness of the background in Fig. 1b is proportional to the amplified spontaneous emission (ASE) in the gain medium. Clearly, the ASE is predominantly polarized along the pump electric field (top image), with substantially no emission being measured with orthogonal polarization (bottom image). This suggests a significant degree of gain anisotropy, which follows from the preferential excitation of molecules with a transition dipole moment parallel to the pump electric field and the rather viscous solvent mixture that inhibits molecular reorientation during the short spontaneous emission lifetime of the dye molecule, $\tau \approx 240$ ps (ref. 37).

The rate of stimulated emission into the LRSPP for a pair of energy levels *a* and *b* is proportional to the dipole moment matrix element $\mathbf{D}_{ab}$ and the electric field of the LRSPP, $\mathbf{E} = [\sim 0, E_y, E_z]$, and has the following form[38]:

$$W_{ab} \propto |\mathbf{E} \cdot \mathbf{D}_{ab}|^2 \quad (1)$$

Because of the inhibited molecular reorientation, excited molecules have dipole moments oriented predominantly in the (*x*, *z*)-plane for

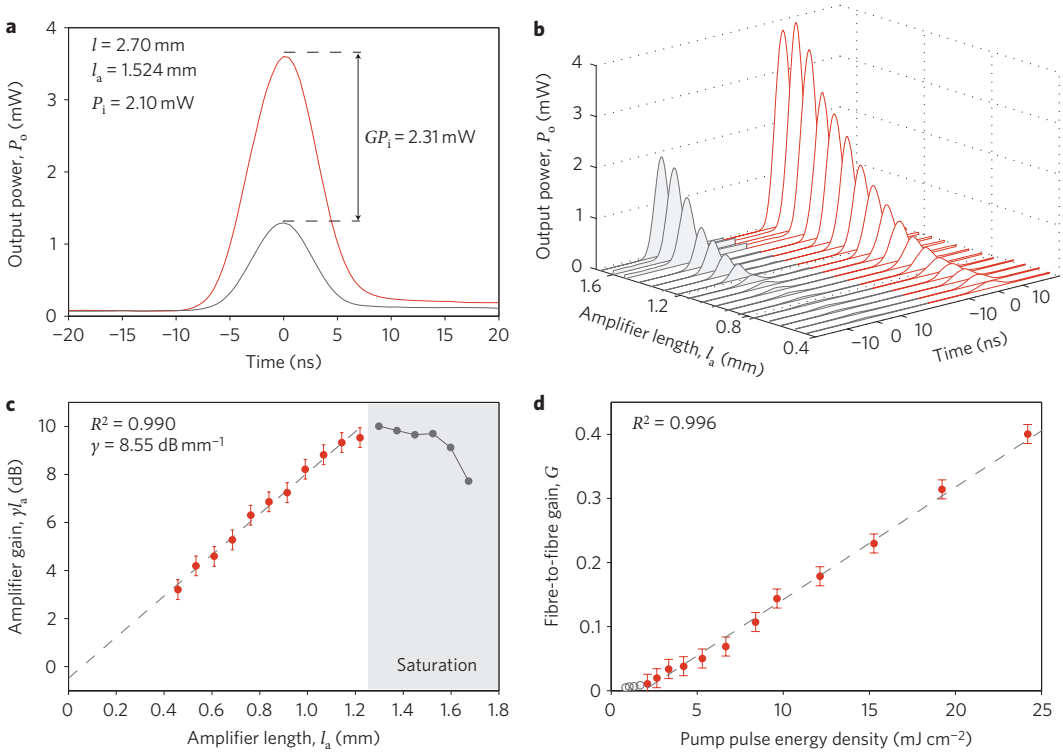

Figure 2 | Active operation. a, Instantaneous power of the amplified probe signal ($P_o = GP_i + \eta$) coupled out of a 2.70-mm-long structure with amplifier length $l_a = 1.524$ mm. The red and grey curves correspond to P_o and η, respectively. The pump energy density and input probe power are set to $E_p = 20 \pm 5$ mJ cm^{-2} and $P_i = 2.10$ mW, respectively. **b**, Measurements of P_o and η as a function of the amplifier length l_a, under the same pump and probe conditions as **a**. **c**, Measurements of amplifier gain versus amplifier length. A linear fit to the unsaturated data yields an LRSPP mode power gain of $\gamma = 8.55$ dB mm^{-1} (error bar, ± 0.412 dB). **d**, Measurements of fibre-to-fibre gain G as a function of the pump energy density for a structure with $l = 2.70$ mm and $l_a = 1$ mm using an input power of $P_i = 0.7$ mW. The linear fit to the data yields an error bar of ± 0.0149.

a normally incident pump of any polarization. For the chosen pump polarization (Fig. 1c), the dot product in equation (1) suggests that LRSPP stimulated emission occurs mainly through the weak E_z field component of the mode, which is approximately two orders of magnitude smaller than E_y (see Supplementary Information). However, as the pump intensity increases, the degree of gain anisotropy is reduced, allowing a stronger interaction of E_y with the gain medium[39,40]. For instance, following the model for an ensemble of randomly oriented rigid dipoles[40], we estimate that for the maximum pump intensity used in our experiments the gain along the y-axis at the surface of the dye layer is ~40% of that along the z-axis.

Passive operation. The passive operation of typical structures was verified before the amplification experiments by measuring the intrinsic mode power attenuation, α_i and the coupling loss per facet C_f by means of cutback[36] at the probe wavelength. Insertion loss measurements were performed on several samples of different lengths using the solvent mixture without dye molecules as the upper cladding to exclude losses due to the ground-state absorption of molecules at λ_e. The measured values of $\alpha_i = 3.06$ dB mm^{-1} and $C_f = 0.360$ dB agree well with theoretical results ($\alpha_i = 3.24$ dB mm^{-1} and $C_f = 0.316$ dB; see Supplementary Information). The low coupling loss guarantees that 92% of the probe power is coupled into the LRSPP. The remaining 8% is reflected, coupled into short-range SPPs (SRSPPs)[30] or coupled into radiation modes. The LRSPP intensity distribution is fairly circular, and its diameter is estimated numerically as ~2.5 μm (see Supplementary Information).

Active operation. During the pump pulse, the structure is composed of three sections defined by the reference planes z_n ($n = 0, 1, 2, 3$) in Fig. 1c. The amplifier section is delimited by the pump beam spot, which covers the region $z_1 < z < z_2$, while two lossy sections, one preceding ($z_0 < z < z_1$) and one following ($z_2 < z < z_3$) the amplifier, are delimited by the unpumped regions. The LRSPP propagates in the $+z$-direction with a complex phase of the form $\exp[(-i\beta + \kappa_n)(z - z_n)]$, where κ_n and β are the field gain ($\kappa_0 = \kappa_2$ being negative) and phase constants, respectively ($e^{i\omega t}$ time-harmonic form assumed). The latter is independent of z, because the real part of the dye refractive index is practically invariant along the structure[37]. Also, for this reason, coupling losses at the planes $z = z_1$ and $z = z_2$ are negligible. The fibre-to-fibre gain expressed in decibels is then given by

$$G_{dB} = \gamma l_a - \alpha_u (l - l_a) - 2C_f \qquad (2)$$

where l_a is the amplifier length, $\gamma = 20\log_{10}(e)\kappa_1$ is the mode power gain due to stimulated emission in the amplifier section, and $\alpha_u = -20\log_{10}(e)\kappa_0$ is the mode power attenuation in the unpumped regions. The latter is larger than α_i due to the ground-state absorption of dye molecules at λ_e.

The power coupled out of the structure (in watts) is given by $P_o = GP_i + \eta$, where P_i is the power delivered by the input fibre, G is the linear fibre-to-fibre gain, and η is the spontaneous emission noise power captured by the output fibre. Figure 2a shows P_o measured with a calibrated a.c.-coupled photoreceiver (see Methods) averaged over 25 pump pulses. The pump pulse energy density is $E_p = 20 \pm 5$ mJ cm^{-2} and the waveguide and amplifier lengths are $l = 2.70$ mm and $l_a = 1.524$ mm, respectively. The grey curve is measured with $P_i = 0$ and corresponds to η. It arises mainly from spontaneous emission into radiation modes (see next section) that fall within the numerical aperture (NA = 0.12) of the fibre integrated over the full emission spectrum of the IR140 dye

molecule, spanning from 850 nm to 930 nm. The red curve is obtained with $P_i = 2.10$ mW. The increment between the two curves represents the amplified mode power GP_i, from which G is obtained straightforwardly. Observe that for this case $GP_i = 2.31$ mW, which yields $G = 1.10$. This indicates not only complete compensation of the losses of the structure (that is, intrinsic mode propagation loss, coupling loss due to both facets and loss due to dye ground-state absorption in the unpumped sections), but also a power gain of 10%. Gain measurements were performed on the same structure for several amplifier lengths over the range $0.457 \leq l_a \leq 1.676$ mm in increments of 0.0762 mm while maintaining the same input power and pump energy density. The resulting curves are shown in Fig. 2b as a function of l_a.

The gain γl_a of the amplifier section is deduced from equation (2) using the fibre-to-fibre gain measurements in Fig. 2b and measured values of C_f (passive operation section) and α_u. The dye behaves as a saturable absorber at λ_e and can present variations due to instabilities during the measurements. To obtain accurate values of α_u, the passive insertion loss $(\alpha_u l + 2C_f)$ of the structure is measured *in situ* simultaneously with each of the gain measurements (see Methods). We obtained a value of $\alpha_u = 7.4$ dB mm^{-1} that decreased monotonically by ~0.5 dB mm^{-1} over the duration of the measurements (~5 min). This could be attributed to a slight blueshift in the absorption spectrum caused by photochemical modifications of dye molecules by both pump and probe radiation, probably due to the small volume (~50 μl) and static conditions of the dye solution. The measured amplifier gain is plotted in Fig. 2c as a function of l_a. The linear amplification region is determined as $0 \leq l_a \leq 1.22$ mm by fitting a linear model to data points, adding l_a incrementally from the smallest value until the goodness of fit (as measured by the Pearson product–moment correlation coefficient R^2) began to degrade substantially. The red data points (Fig. 2c) were selected in this manner to participate in the linear model, whereas the grey ones were deemed to fall within the non-linear region of the amplifier. The slope of the linear model yields $\gamma = 8.55$ dB mm^{-1}, with error bars of ± 0.412 dB and $R^2 = 0.990$. The coupling loss at the amplifier interfaces (planes z_1 and z_2) is obtained as the intercept, yielding 0.48 dB. This deviation from the expected value of zero is comparable to the experimental error. Clearly, for $l_a > 1.22$ mm, the amplifier gain is not linear; this is attributed mainly to mode gain saturation.

A signature of stimulated emission is the linear (unsaturated) gain behaviour as a function of the pump energy density E_p. To strengthen the observation of stimulated emission into the LRSPP, fibre-to-fibre gain (G) measurements are plotted in Fig. 2d as a function of E_p, while maintaining a fixed amplifier length of $l_a = 1$ mm (for the 2.70-mm-long structure) and constant input power of $P_i = 0.7$ mW. Gain measurements for $E_p \leq 2$ mJ cm^{-2} (open circles) fall below the noise level of our detection system. For larger values of E_p the linearity of G is supported by an excellent linear fit with $R^2 = 0.996$. No saturation effects are observed within the measurement range of $2 < E_p < 24.5$ mJ cm^{-2}.

Reduced spontaneous emission noise. In a plasmonic amplifier, the spontaneous emission exhibits a complex behaviour due to a variety of energy decay channels engendered by the metal[42–44]. For the structure investigated here, these decay channels include spontaneous emission into the radiation modes of the structure, spontaneous emission into the LRSPP and SRSPP modes, and coupling to electron–hole pairs in the metal film, where the energy is directly transferred from the molecule to carriers in the metal by means of a dipole–dipole interaction. Excited molecules preferentially relax through specific decay channels depending on their distance from the metal and their dipole–moment orientation. To illustrate this phenomenon, we consider for simplicity the one-dimensional variant of the structure in Fig. 1a

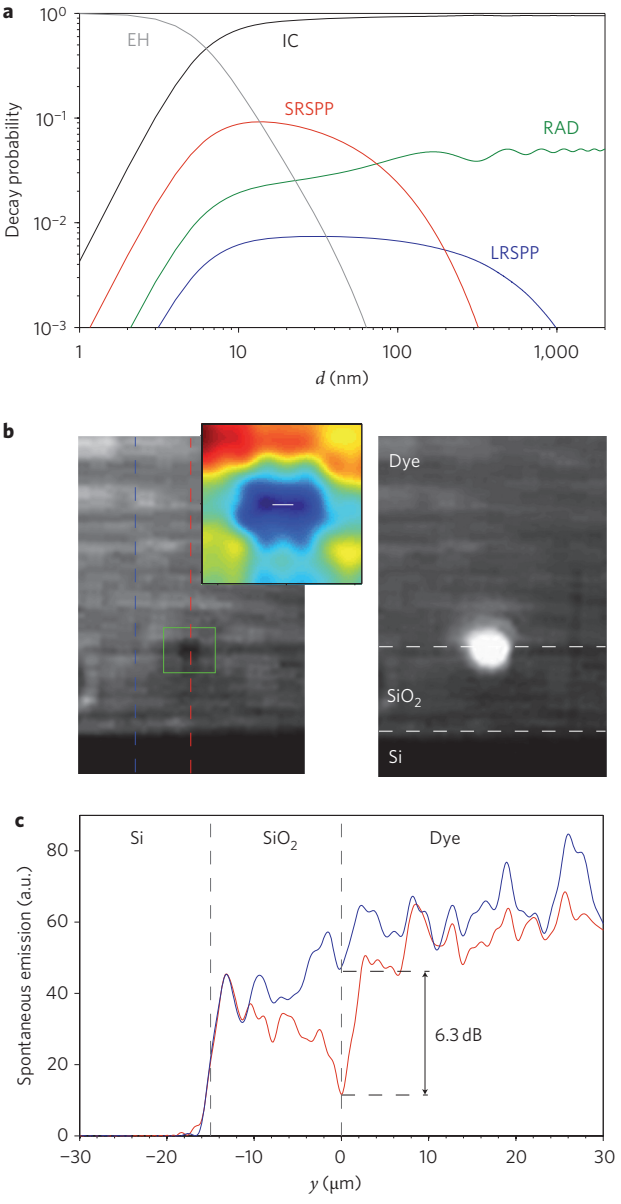

Figure 3 | Reduced spontaneous emission. a, Decay probability of isotropically oriented dipoles near a metal slab into various channels calculated for the one-dimensional variant of the structure on Fig. 1a. **b**, Light collected from the output facet of a structure pumped with *z*-polarized light. Left image, probe off; right image; probe on. The inset shows the intensity distribution (in false colour scale) near the 1-μm-wide metal stripe (indicated by the white line). **c**, Spontaneous emission intensity distribution in arbitrary units along the vertical cuts indicated by the red and blue dashed lines in **b** (left). EH, electron–hole pair; IC, internal conversion; SRSSP, short-range surface plasmon-polarition; RAD, radiative modes.

(infinite metal stripe width) with a semi-infinite gain medium formed of isotropically excited dipoles. The decay probabilities are shown in Fig. 3a as a function of molecule–metal separation d. These curves are computed using the classical theory of molecular fluorescence near a metal (see Methods). Molecules relax mainly via non-radiative channels, that is, through internal conversion for $d > 5$ nm due to the low quantum efficiency of IR140 ($\phi \approx 0.05$) and through coupling to electron–hole pairs in the metal for $d < 5$ nm. The remaining channels involve spontaneous emission into modes of the structure (LRSPP, SRSPP and radiative modes, RAD) and contribute to the optical noise of

the amplifier. Note that spontaneous emission into the SRSPP is the dominant decay channel for $d < 100$ nm, being 10 and 5 times more probable than decay into the LRSPP and RAD channels, respectively. For $d > 100$ nm, the RAD channel dominates, being at least 5 times more probable than decay into the LRSPP channel.

Consider now Fig. 3b, which shows images of light collected from the output facet of a structure with $l = 1.8$ mm and $l_a = 1.05$ mm while being pumped by z-polarized light. The images on the left and right correspond to cases where the probe signal is turned off and on, respectively. The background fluorescence is randomly polarized, as expected from a collection of excited molecules with a symmetrical dipole–moment distribution about the z-axis[41]. From the image on the left, a significant reduction of spontaneous emission is observed near the metal stripe compared to the background. The inset enlarges this region, scaling the light intensity in false colour. Figure 3c shows the spontaneous emission intensity distribution along the two cuts indicated by the vertical dashed lines in Fig. 3b (left). The red curve corresponds to the cut approximately through the centre of the metal stripe and the blue curve corresponds to a cut shifted approximately 10 μm to the left of the metal stripe. The latter corresponds to spontaneous emission into radiation modes; molecules are distant enough from the metal stripe that their fluorescence is not affected. The spontaneous emission reduction relative to the emission in the bulk is 6.3 dB, as given by the difference between the two curves at $y \approx 0$. These curves are obtained from a diffraction-limited image, so the low-intensity region is blurred by the surrounding light. The measured reduction is therefore probably underestimated.

These measurements could be explained qualitatively by elements of the decay calculations shown in Fig. 3a. First, the spontaneous emission probability into the LRSPP is much smaller than that of the main radiative decay channels near the metal. The LRSPP therefore conveys little spontaneous emission to the output facet. Second, the probability of spontaneous emission into radiative modes is considerably reduced close to the metal. Third, the large emission into the SRSPP is quickly absorbed by the metal (through high modal loss), so the SRSPP also conveys little emission to the output facet. Finally, the fluorescence quenching caused by coupling to electron–hole pairs in the metal also reduces the spontaneous emission; however, it affects only a small region near the metal.

The gain and low spontaneous emission noise into the LRSPP are important attributes of this class of amplifier. Furthermore, the large spontaneous emission into the SRSPP combined with its large propagation loss equips the amplifier with an efficient quenching mechanism of guided noise. These attributes suggest the possibility of low-noise optical amplification through the LRSPP, provided that the LRSPP can be isolated from the unguided noise carried by the radiation modes of the structure.

Methods

Experimental set-up. For the amplification measurements the active waveguide structure was mounted on a thermo-electric cooling device to stabilize the temperature of the dye solution to 23 °C and avoid refractive index fluctuations due to thermo-optic effects. The active waveguide was also enclosed in a nitrogen capsule to provide the dry environment necessary to stabilize the hygroscopic dye solution. The pump light, consisting of 8-ns (FWHM) pulses with a repetition rate of 10 Hz, was generated with a frequency-doubled Nd:YAG pumped dye laser (Spectra-Physics Mod. Quanta-Ray Lab10/Cobra-Stertch). The energy and polarization of the pump beam were controlled with a $\lambda/2$ wave plate followed by a Glan-Laser polarizer, and its spot size, which defines the amplifier section was carefully controlled with a micrometre driven variable slit.

For both passive (without dye molecules and with unpumped dye molecules) and active measurements, a tuneable c.w. Ti:sapphire laser (Spectra-Physics Mod. 3900 CW) coupled to a panda-type polarization-maintaining (PM) fibre (Thorlabs Mod. PM780-HP) was used to generate the probe signal. This was then passed through a 10-dB PM fibre splitter, which was used to monitor the input power in real time during the measurements. The LRSPP was coupled in and out of the structure via end-fire coupling using the same type of PM fibre. Both fibres were mounted on five-axis micropositioners and carefully aligned to the waveguide structure in terms of position and polarization. Light collected by the output fibre was collimated and passed through a TM polarizer to remove residual transverse electric (TE) light. A 3-dB splitter then divided the signal into two branches, one of which delivered the signal to a calibrated a.c.-coupled fast photoreceiver (Newport Mod. 818-BB-21A) to perform the gain measurements. The photoreceiver was monitored with a radio-frequency oscilloscope, which in turn was synchronized to the 10-Hz pump signal. All gain measurements were averaged over 25 pump pulses to minimize errors due to possible pulse-to-pulse energy variations. The second branch delivered the optical signal to a low-power c.w. photodetector (Newport Mod. 918D-SL), which was used to monitor the insertion loss of the structure during the measurements. Because the amplified signal was only 8 ns in duration, it did not significantly alter the average power of the c.w. component. Hence, the value measured by the low-power c.w. photodetector was used to compute the passive insertion loss (unpumped) of the structure, given by $\alpha_u l + 2C_F$.

For the measurements of gain anisotropy and reduced spontaneous emission, the light intensity distribution at the output facet of the structure was imaged onto a vidicon-type infrared camera (Electrophysics Mod. MicronViewer 7290) equipped with an 808-nm blocking filter using a ×20 microscope objective. Gain anisotropy was measured by placing a polarization filter before the camera to visualize the spontaneous emission with a particular electric field component; no polarization filter was used for the measurement of reduced spontaneous emission. For both measurements, the camera recorded images over a long time interval, capturing the dye spontaneous emission and LRSPP intensities at a frame rate of 50 Hz. Images presented throughout the paper correspond to video frames where the recorded spontaneous emission is maximum. Images were corrected for the background intensity (ambient light) by subtracting from every pixel of an image the grey-scale value of the bottom pixel in the silicon layer. Because silicon absorbs efficiently over the emission spectrum of the dye, the subtracted value does not affect the spontaneous emission level.

Numerical techniques. The probabilities of energy decay into the different channels in the vicinity of the metallic film were obtained following the classical theory of molecular fluorescence near metallic surfaces; refs 42–44 provide a comprehensive discussion of the theory. The material refractive indices used in our simulations are those used for modelling the passive structure (see Supplementary Information). To account approximately for electron screening in the metal (which becomes important only when the distance between the molecule and the metal is a few nanometres) we considered only dipole field components with in-plane wave vectors $k_{\|}$ within the electron–hole excitation continuum of gold at λ_e; that is, $k_{\|} < (2m_e\omega_e/\hbar + k_F^2)^{1/2} + k_F$, where k_F is the Fermi wave vector, $\hbar$ is the reduced Planck's constant, m_e is the electron mass and ω_e is the angular frequency of light.

Received 3 September 2009; accepted 17 February 2010; published online 28 March 2010

References

1. Raether, H. *Surface Plasmons on Smooth and Rough Surfaces and on Gratings* (Springer, 1988).
2. Barnes, W. L., Dereux, A. & Ebbesen, T. W. Surface plasmon subwavelength optics. *Nature.* **424,** 824–830 (2003).
3. Shalaev, V. M. Optical negative-index metamaterials. *Nature Photon.* **1,** 41–48 (2007).
4. Kawata, S., Inouye, Y. & Verma, P. Plasmonics for near-field nano-imaging and superlensing. *Nature Photon.* **3,** 388–394 (2009).
5. Anker, J. N. *et al.* Biosensing with plasmonic nanosensors. *Nature Mater.* **6,** 442–453 (2008).
6. Bergman, D. J. & Stockman, M. I. Surface plasmon amplification by stimulated emission of radiation: quantum generation of coherent surface plasmons in nanosystems. *Phys. Rev. Lett.* **90,** 027402 (2003).
7. Nezhad, M. P., Tetz, K. & Fainman, Y. Gain assisted propagation of surface plasmon polaritons on planar metallic waveguides. *Opt. Express.* **12,** 4072–4079 (2004).
8. Avrutsky, I. Surface plasmons at nanoscale relief gratings between a metal and a dielectric medium with optical gain. *Phys. Rev. B.* **70,** 155416 (2004).
9. Okamoto, T., H'Dhili, F. & Kawata, S. Towards plasmonic band gap laser. *Appl. Phys. Lett.* **85,** 3968–3970 (2004).
10. Maier, S. A. Gain-assisted propagation of electromagnetic energy in subwavelength surface plasmon polariton gap waveguides. *Opt. Commun.* **258,** 295–299 (2006).
11. Winter, G., Wedge, S. & Barnes, W. L. Can lasing at visible wavelength be achieved using the low-loss long-range surface plasmon–polariton mode? *New J. Phys.* **8,** 125 (2006).
12. Alam, M. Z., Meier, J., Aitchison, J. S. & Mojahedi, M. Gain assisted surface plasmon polariton in quantum well structures. *Opt. Express.* **15,** 176–182 (2007).
13. De Leon, I. & Berini, P. Theory of surface plasmon–polariton amplification in planar structures incorporating dipolar gain media. *Phys. Rev. B.* **78,** 161401(R) (2008).
14. De Leon, I. & Berini, P. Modeling surface plasmon–polariton gain in planar metallic structures. *Opt. Express.* **17,** 20191–20202 (2009).

15. Seidel, J., Grafstrom, S. & Eng, L. Stimulated emission of surface plasmons at the interface between a silver film and an optically pumped dye solution. *Phys. Rev. Lett.* **94,** 177401 (2005).
16. Noginov, M. A. *et al.* Compensation of loss in propagating surface plasmons polariton by gain in adjacent dielectric medium. *Opt. Express.* **16,** 1385–1392 (2008).
17. Noginov, M. A. *et al.* Stimulated emission of surface plasmon polaritons. *Phys. Rev. Lett.* **101,** 226806 (2008).
18. Ambati, M. *et al.* Observation of stimulated emission of surface plasmon polaritons. *Nano Lett.* **8,** 3998–4001 (2008).
19. Grandidier, J. *et al.* Gain-assisted propagation in a plasmonic waveguide at telecom wavelength. *Nano Lett.* **9,** 2935–2939 (2009).
20. Oulton, R. F. *et al.* Plasmon lasers at deep subwavelength scale. *Nature.* **461,** 629–632 (2009).
21. Hill, M. T. *et al.* Lasing in metallic-coated nanocavities. *Nature Photon.* **1,** 589–594 (2007).
22. Hill, M. T. *et al.* Lasing in metal–insulator–metal sub-wavelength plasmonic waveguides. *Opt. Express.* **17,** 11107–11112 (2009).
23. Noginov, M. A. *et al.* Demonstration of a spaser-based nanolaser. *Nature.* **460,** 1110–1113 (2009).
24. Kovacs, G. J. Optical excitation of surface plasma waves in an indium film bounded by dielectric layers. *Thin Solid Films* **60,** 33–44 (1979).
25. Fukui, M. *et al.* Lifetimes of surface plasmons in thin silver films. *Phys. Stat. Sol. B.* **91,** K61–K64 (1979).
26. Sarid, D. Long-range surface-plasma waves on very thin metal films. *Phys. Rev. Lett.* **47,** 1927–1930 (1981).
27. Burke, J. J., Stegeman, G. I. & Tamir, T. Surface-polariton-like waves guided by thin, lossy metal films. *Phys. Rev. B.* **33,** 5186–5201 (1986).
28. Yang, F., Sambles, J. R., & Bradberry, G. W. Long-range surface modes supported by thin films. *Phys. Rev. B.* **44,** 5855–5872 (1991).
29. Berini, P. Long-range surface plasmon polaritons. *Adv. Opt. Photon.* **1,** 484–588 (2009).
30. Berini, P. Plasmon–polariton waves guided by thin lossy metal films of finite width: bound modes of symmetric structures. *Phys. Rev. B.* **61,** 10484–10503 (2000).
31. Jette-Charbonneau, S., Charbonneau, R., Lahoud, N., Mattiussi, G. & Berini, P. Bragg gratings based on long-range surface plasmon-polariton waveguides: comparison of theory and experiment. *IEEE J. Quantum Electron.* **98,** 1480–1491 (2005).
32. Bozhevolnyi, S. I., Boltasseva, A., Sondergaard, T., Nikolajsen, T. & Leosson, K. Photonic bandgap structures for long-range surface plasmon polaritons. *Opt. Commun.* **250,** 328–333 (2005).
33. Charbonneau, R. *et al.* Passive integrated optics elements based on long-range surface plasmon polaritons. *J. Lightwave Technol.* **24,** 477–494 (2006).
34. Boltasseva, A. *et al.* Integrated optical components utilizing long-range surface plasmon polaritons. *J. Lightwave Technol.* **23,** 413–422 (2005).
35. Berini, P. Bulk and surface sensitivities of surface plasmon waveguides. *New J. Phys.* **10,** 105010 (2008).
36. Berini, P., Charbonneau, R., Lahoud, N. & Mattiussi, G. Characterization of long-range surface-plasmon-polariton waveguides. *J. Appl. Phys.* **98,** 043109 (2005).
37. Sperber, P., Spangler, W., Meier, B. & Penzkofer, A. Experimental and theoretical investigation of tunable picosecond pulse generation in longitudinally pumped dye laser generators and amplifiers. *Opt. Quantum Electron.* **20,** 395–431 (1988).
38. Bransden, B. H. & Joachain, C. J. *Physics of Atoms and Molecules* (Longman, 1983).
39. Mourou, G. & Denariez, M. M. Polarization of fluorescence and bleaching of dyes in a high-viscosity solvent, *IEEE J. Quantum Electron.* **QE9,** 787–790 (1973).
40. Reyzer, K. C. & Casperson, L. W. Polarization characteristics of dye-laser amplifiers II. Isotropic molecular distribution. *J. Appl. Phys.* **51,** 6083–6090 (1980).
41. Valeur, B. *Molecular Fluorescence, Principles and Applications* (Wiley-VCH, 2002).
42. Chance, R. R., Prock, A. & Silbey, R. Molecular fluorescence and energy transfer near interfaces. *Adv. Chem. Phys.* **37,** 1–65 (1978).
43. Ford, G. W. & Weber, W. H. Electromagnetic interactions of molecules with metal surfaces. *Phys. Rep.* **113,** 195–287 (1984).
44. Barnes, W. L. Fluorescence near interfaces: the role of photonic mode density. *J. Mod. Opt.* **45,** 661–699 (1998).

Acknowledgements

The authors thank Prof. J.C. (Tito) Scaiano, M. Grenier, and other members of the photochemistry laboratory at the University of Ottawa for their assistance in measuring the IR140 absorption spectrum. This work was generously supported by the Natural Sciences and Engineering Research Council of Canada.

Author contributions

I.D.L. carried out the experimental work, performed the theoretical analysis, and prepared the manuscript. P.B. directed the project and contributed to the manuscript preparation. I.D.L and P.B. designed the experiments and the set-up, and analysed and interpreted the experimental results.

Additional information

The authors declare no competing financial interests. Supplementary information accompanies this paper at www.nature.com/naturephotonics. Reprints and permission information is available online at http://npg.nature.com/reprintsandpermissions/. Correspondence and requests for materials should be addressed to P.B.